Chemical, microphysical, and optical properties of polar stratospheric clouds

J. Schreiner,[1] C. Voigt,[1] C. Weisser,[1] A. Kohlmann,[1] K. Mauersberger,[1] T. Deshler,[2] C. Kröger,[2] J. Rosen,[2] N. Kjome,[2] N. Larsen,[3] A. Adriani,[4] F. Cairo,[4] G. Di Donfrancesco,[4,5] J. Ovarlez,[6] H. Ovarlez,[6] and A. Dörnbrack[7]

Received 9 May 2001; revised 21 March 2002; accepted 25 March 2002; published 7 December 2002.

[1] A balloonborne gondola for a comprehensive study of polar stratospheric clouds (PSCs) was launched on 25 January 2000 near Kiruna/Sweden. Besides an aerosol composition mass spectrometer, the gondola carried optical particle counters, two backscatter sondes, a hygrometer, and several temperature and pressure sensors. A mountain wave induced PSC was sampled between 20 and 23 km altitude. Strongly correlated PSC particle properties were detected with the different instruments. A large variability of particle types was measured in numerous PSC layers, and PSC development was followed for about two hours. Liquid ternary PSC layers were found at temperatures near the ice frost point. A large fraction of the sampled cloud layers consisted of nitric acid trihydrate (NAT) particles with a molar ratio H_2O:HNO_3 close to 3 at temperatures near and below the equilibrium temperature T_{NAT}. The median radius of the NAT particle size distribution was between 0.5 and 0.75 μm at concentrations around 0.5 cm^{-3}. Below the NAT layers and above T_{NAT}, thin cloud layers containing a few large particles with radii up to 3.5 μm coexisted with smaller solid or liquid particles. The molar ratio in this region was found to be close to two. *INDEX TERMS:* 0305 Atmospheric Composition and Structure: Aerosols and particles (0345, 4801); 0320 Atmospheric Composition and Structure: Cloud physics and chemistry; 0340 Atmospheric Composition and Structure: Middle atmosphere—composition and chemistry; *KEYWORDS:* polar stratospheric clouds, aerosol properties, ozone hole, nitric acid trihydrates, aerosol composition analysis

Citation: Schreiner, J., et al., Chemical, microphysical, and optical properties of polar stratospheric clouds, *J. Geophys. Res.*, *107*, 8313, doi:10.1029/2001JD000825, 2002. [printed *108*(D5), 2003]

1. Introduction

[2] The analysis of springtime polar ozone destruction and the prediction of future ozone trends require a detailed knowledge of the size, composition, and phase of polar stratospheric cloud particles. PSCs form in the winter polar stratosphere through condensation of mainly water and nitric acid onto preexisting sulfate aerosols at temperatures below 200 K. In situ measurements [*Fahey et al.*, 1989; *Dye et al.*, 1990] and model calculations [*Carslaw et al.*, 1994; *Tabazadeh et al.*, 1994] indicate that H_2O and HNO_3 can be present in various concentrations in PSC particles, which influence their microphysical and optical properties. Therefore a classification into different particle types has been established [*Browell et al.*, 1990; *Toon et al.*, 1990; *Koop et al.*, 1997].

[3] The existence of solid nitric acid trihydrate (NAT) particles in PSCs at temperatures above the ice frost point was predicted by *Crutzen and Arnold* [1986] as well as by *Toon et al.* [1986] and later confirmed in laboratory measurements of *Hanson and Mauersberger* [1988]. In the polar stratosphere, NAT particles were only recently found by direct particle composition measurements [*Voigt et al.*, 2000a] at temperatures below the NAT threshold T_{NAT}. A further analysis of those measurements is presented here. Indirect evidence for NAT was first established by *Fahey et al.* [1989] and later supported through optical particle characterization [*Carslaw et al.*, 1998; *Toon et al.*, 2000]. The presence of solid nitric acid dihydrate (NAD) particles at temperatures 2 to 3 K below T_{NAT} has been suggested [*Worsnop et al.*, 1993], although their existence has not been confirmed in the stratosphere. The formation of liquid ternary aerosols (LTA) at temperatures 3 to 4 K below T_{NAT}, predicted by model calculations [*Carslaw et al.*, 1994; *Tabazadeh et al.*, 1994; *Drdla et al.*, 1994; *Del Negro et al.*, 1997], has been experimentally verified by

[1]Division of Atmospheric Physics, Max-Planck-Institute for Nuclear Physics, Heidelberg, Germany.
[2]Department of Atmospheric Science, University of Wyoming, Laramie, Wyoming, USA.
[3]Division of Middle Atmospheric Research, Danish Meteorological Institute, Copenhagen, Denmark.
[4]Istituto per la Scienza dell'Atmosfera e del Clima, Rome, Italy.
[5]Ente per le Nuove Tecnologie, l'Energia e l'Ambiente, Sezione Clima, La Casaccia Research Center, Rome, Italy.
[6]Laboratoire de Meteorologie Dynamique, Palaiseau, France.
[7]Institute for Physics of the Atmosphere, Deutsches Zentrum für Luft- und Raumfahrt Oberpfaffenhofen, Wessling, Germany.

0148-0227/02/2001JD000825$09.00

PSC composition analysis [*Schreiner et al.*, 1999b; *Voigt et al.*, 2000b] and optical particle measurements [*David et al.*, 1997; *Del Negro et al.*, 1997; *Larsen et al.*, 2000]. Whereas the formation processes and the composition of PSCs at temperatures above the frost point (type I PSCs) is still under debate [*World Meteorological Organization* (*WMO*), 1999], it is generally accepted that ice particles (type II PSCs) exist below the frost point [*Dye et al.*, 1990]. A few particles grow to sizes large enough for sedimentation, transporting significant amounts of water (dehydration) [*Fahey et al.*, 1990; *Schiller et al.*, 2002] and nitric acid (denitrification) [*Fahey et al.*, 2001] out of the lower stratosphere. This enhances, through removal of reactive nitrogen compounds, the potential for ozone destruction.

[4] Warmer conditions in the North polar stratosphere compared to the Antarctic stratosphere can lead to incomplete halogen processing, which limits the size of the ozone hole above the Arctic compared to the Antarctic [*WMO*, 1999]. The development of mesoscale cold temperature regions induced by adiabatic expansion of air in mountain waves is of particular importance in the Arctic at temperatures near the PSC threshold. Under these conditions, mountain waves can lead to particle formation in regions where synoptic temperature predictions are too high for the presence of PSCs [*Carslaw et al.*, 1999]. Therefore, in the Northern Hemisphere, the timescales and the extent of halogen processing with subsequent ozone depletion strongly depend on meteorological conditions and on the stability and composition of PSC particles [*Carslaw et al.*, 1998]. This paper describes results from a balloon flight that was dedicated to mountain wave PSC investigations. After a brief introduction to the instruments carried on the balloon gondola, a detailed analysis of the combined measurements will be presented.

2. Instrumentation of the Gondola

[5] A sketch of the instruments assembled on the balloon gondola to perform a comprehensive analysis of chemical, physical and optical properties of PSC particles are shown in Figure 1. The instrumentation consisted of an aerosol composition mass spectrometer (ACMS), three optical particle counters (OPCs), a laser and a white light backscatter sonde, a dew point hygrometer and several temperature and pressure sensors. The concept of operation and performance of each instrument is briefly described below; for the ACMS, however, additional experimental and performance details are presented.

2.1. Aerosol Composition Mass Spectrometer

[6] A crucial part of the ACMS system is a particle-focusing device called an aerodynamic lens, which is a small metal cylinder with a sequence of orifices inside [*Schreiner et al.*, 1998, 1999a]. PSC particles travel with ambient air through the lens when it is opened to the atmosphere above 18 km (below 100 mbar). Inside, particles are focused to the centerline, and at its exit a very narrow beam will leave. Dimensions of the orifices are such that particles with equivalent spherical radii between 0.05 μm and about 1 μm are focused with a transmission efficiency between 80 and 95% at pressures between 25 and 45 mbar. That covers the pressure range in which different PSC layers were encountered during the balloon flight reported in this paper. Smaller particles just follow the streamlines of the gas molecules and will not be focused, while the detection of larger particles is prevented because they may not enter the lens or impact somewhere inside the lens due to their moment of inertia. During a flight the gas flow through the lens is about 1 l min^{-1}. The lens, exposed to the outside, is near ambient temperature. Calculations with a nonequilibrium model of *Meilinger et al.* [1995] indicate that the composition change of liquid ternary aerosols and NAT particles is negligible for the short time that the particles are inside the lens and traveling within the vacuum system [*Voigt*, 2000]. In addition to many laboratory tests [*Schreiner et al.*, 1998], valuable experience has been gained from the operation of such a lens in large aerosol chamber experiments with binary and ternary solution particles [*Zink et al.*, 2002].

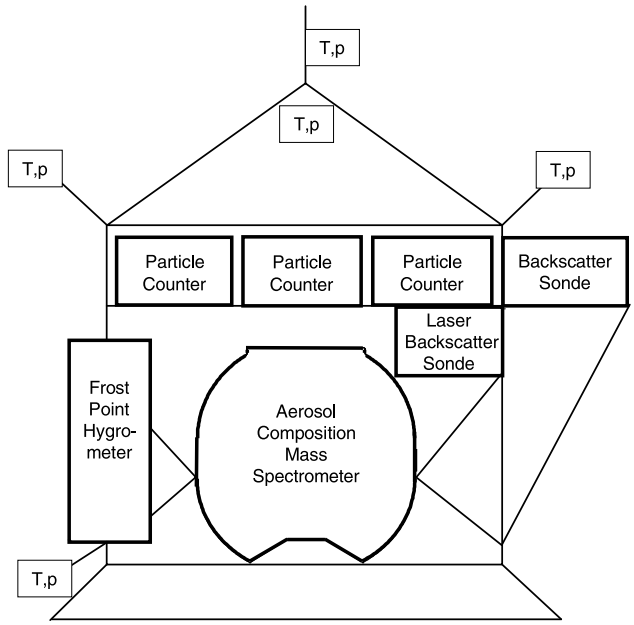

Figure 1. Schematic of instruments assembled on the balloon gondola for a comprehensive analysis of PSC particle properties.

[7] After the aerodynamic lens, ambient gas molecules will spread out, and most of the molecules will be removed by a liquid helium pump. The particle beam will continue unaffected through a narrow opening into a second chamber that contains another liquid helium pump. Within that second chamber the particles enter a small heated evaporation sphere and vaporize. Most of the evolved gases (mainly H_2O and HNO_3) will leave the sphere toward the ionizing electron beam of the mass spectrometer. The ionized molecules are drawn into a magnetic instrument for mass analysis. The combination of the two liquid helium pumps provides a large enrichment of condensed phase species over ambient gases without altering particle composition. The aerosol beam can be blocked for gas background measurements. Before opening the instrument to the atmosphere and before the first encounter with cloud particles, additional gas background checks can be made for H_2O and

HNO_3 as well as for other gases. Periods of low aerosol volume during the flight again serve to estimate residual gases.

[8] Based on laboratory tests and on the measured count rates of H_2O when traveling through cloud layers, particles with radii larger than 1.25 μm were probably not focused and those larger than 1.5 μm were not focused at all at 25 mbar and higher. Although the mass spectrometer detector was designed to measure the H_2O and HNO_3 content of PSC particles of much larger radii, no high count rates were observed. It must be recognized that only those particles which are focused and thus enter the small sphere in the second chamber will evaporate and produce signals in H_2O and HNO_3 above the background. Overall, it was found (after evaluating focusing properties and instrument stability) that the mass spectrometer performed well throughout the flight. The signals of H_2O at mass 18 and of HNO_3 at 63 and 46 (NO_2^+, fragmented in the ion source from HNO_3) extended well above the instrument background levels. Increases and decreases of mass spectrometer signals correlated well with particle parameters measured by other instruments onboard the gondola.

[9] The main objective of the ACMS experiment is to obtain molar ratios of H_2O and HNO_3 in PSC particles. The evaporating particles will produce gas pulses inside the small gold sphere, which will result in relatively steady mass spectrometer signals of H_2O and HNO_3 when many particles are present in the beam while, when only a few particles enter the sphere, spikes are observed. Thus no single particle analysis is possible, although larger particles will produce high count rates particularly in H_2O, indicating, for example, the presence of solid NAT particles. A set of H_2O and HNO_3 data is measured sequentially almost every 2 s. For analysis many single measurements are combined to derive a molar ratio H_2O/HNO_3. Important are the laboratory calibrations before the flight. For H_2O, HNO_3, and HCl, instrument sensitivities with uncertainties of less than 15% were obtained by admitting the three gases in well-known concentrations into the evaporation sphere. For the two species HCl and H_2SO_4 which are present as minor constituents in PSC particles, only upper limits can be given: Chlorine species such as HCl were measured to be less than 0.2 ppbv in the condensed phase, which represents the upper concentration limit. Due to a strong fragmentation of sulfuric acid in the ion source and a long wall adsorption time constant there is a higher detection limit of 0.4 ppbv for sulfuric acid. The amount of sulfuric acid contained in PSCs encountered during the flight is estimated to be less than 0.4 ppbv. The entire ACMS system including experimental details such as testing, calibration, and operation is described by *Schreiner et al.* [2002].

2.2. Optical Particle Counters

[10] Three optical particle counters [*Deshler and Oltmans*, 1998] measured the concentration of condensation nuclei (CN, $r > 0.01$ μm) and optically detectable aerosols ($0.15 < r < 10$ μm). The latter are classified into twelve size classes of which six will be shown. The inlets of the counters were oriented horizontally to avoid any sampling bias on ascent or descent. The size of the particles is calculated from the intensity of scattered white light at 40° from the forward direction using Mie theory for spherical particles and an index of refraction of 1.45 [*Deshler et al.*, 2000]. CN concentrations are measured using ethylene glycol vapor to force the particles to grow to optically detectable sizes. The particle concentration limit for particles with radius >0.15 μm is 5.7×10^{-4} cm^{-3}. The temporal resolution of the OPC data is 10 s.

2.3. Backscatter Sondes

[11] A laser backscatter sonde [*Adriani et al.*, 1998] measured aerosol and molecular scattering at 180° ± 1° within 50 m of the gondola every 2 s using laser pulses at 685 nm (laser diode) and 532 nm (Nd-YAG) wavelengths. The backscatter ratio (BR), the total volume backscatter to the molecular backscatter, is derived with an error <7%. Since the depolarization allows conclusions about the shape of particles, the backscattered laser light at 532 nm is split further into its parallel and perpendicular components. Aspherical particles, and thus solid, show an elevated signal in the depolarization, which is measured with an uncertainty of 10%.

[12] A second backscatter sonde [*Rosen and Kjome*, 1991; *Larsen et al.*, 1997] uses a xenon lamp, emitting a white light flash every 7 s. The light scattered by particles and molecules within few meters from the instrument is monitored with two photodiodes equipped with filters at 480 and 940 nm. The ratio between particle and molecule backscatter (BR) and a color index ($CI = BR940/BR480$) can be derived. In principle, the color index is correlated to the size of the particles. However, in PSCs, when particles are larger than 1 μm in radius, they are normally solid. This permits the extrapolation of the size information toward the phase information.

2.4. Water Vapor and Temperature Measurements

[13] The frost point was measured with a dew point sensor described by *Ovarlez and Ovarlez* [1996], that has an accuracy of 0.3 K. A layer of water ice, condensed on a mirror, is detected by an optical system. The onset of the condensation as a function of mirror temperature represents the frost point (T_{ICE}) of the air passing the mirror. From these measurements the water vapor volume mixing ratio can be determined with an accuracy of 10% [*Ovarlez and Ovarlez*, 1994].

[14] The local atmospheric temperature is a very important parameter for PSC characterization. Therefore four temperature sensors were placed on booms one meter outside the gondola structure and a fifth sensor was placed on the load line two meters above the gondola to minimize interference from the payload (see Figure 1). The different temperature sensor data showed an excellent agreement of better than ±0.5 K over the range 185 to 198 K measured during the flight. For the first time detailed PSC particle analysis can be closely correlated with well-known temperatures at the location of the PSCs.

3. Meteorology

[15] PSC particle formation and existence is strongly controlled by meteorological conditions. In the Arctic winter 1999/2000 the persistence of a large cold polar vortex dominated the stratospheric circulation and led throughout January to synoptical temperatures below the

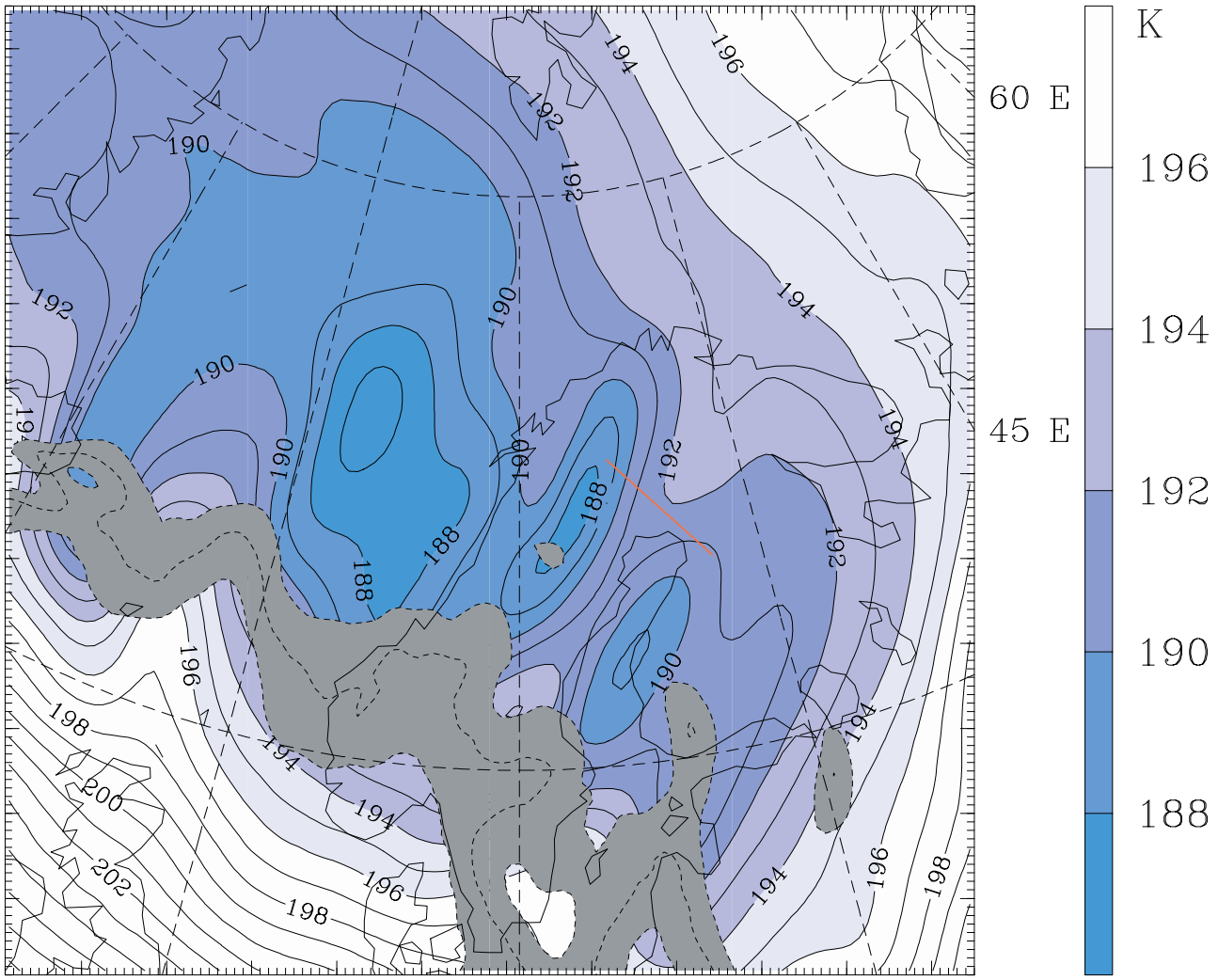

Figure 2. Synoptic stratospheric temperature distribution on 26 January 2000 at 0000 UT. ECMWF-T319 analyzed temperature (in K; shaded blue) and potential vorticity (gray) ($70 \pm 5 \times 10^{-6}$ km^2 s^{-1} kg^{-1}) on the 550 K potential temperature surface. The red line denotes the balloon trajectory.

NAT threshold at the 30 and the 50 mbar level. At the end of January the vortex moved over northern Scandinavia. The edge of the vortex is defined in Figure 2 as a potential vorticity belt of $(70 \pm 5) \times 10^{-6}$ km^2 s^{-1} kg^{-1}, marked by the gray shading. Figure 2 also shows the synoptic temperature on 26 January, 0000 UT on the 550 K potential temperature surface, based on ECMWF-T319 analysis [*Dörnbrack et al.*, 2002]. The center of the cold area with temperatures below the ice frost point was located above and northwest of Scandinavia. The red line indicates the balloon trajectory starting near Kiruna.

[16] Mountain wave activity developed on the 25th and persisted until the 27th January 2000 above northern Scandinavia. Westerly surface winds forced the air over the Scandinavian mountains and this perturbation penetrated into the stratosphere. Strong temperature anomalies, developed through adiabatic expansion of ascending air in mountain waves, led to a nearly stationary cold temperature field in the lower stratosphere. A vertical cross section of the temperature distribution along the flight track on 25 January 2000 at 2200 UT, calculated with a mesoscale meteorological model (MM5) [*Dörnbrack et al.*, 2002], is shown in Figure 3. The upper panel displays a cold trough with temperatures as low as 7 K below the ice frost point directly above the Scandinavian mountains. The balloon trajectory (black line) crossed an extension of this trough at higher temperatures. The lower panel indicates the orography below the balloon trajectory. During the initial ascent of the balloon, temperatures 1 to 2 K below the frost point were measured, increasing to temperatures near T_{NAT} in the latter part of the flight.

[17] Back trajectory calculations, based on ECMWF analysis, for a time period of 20 hours before the encounter show temperatures below T_{NAT}, while 100 hours before the encounter temperatures above T_{SAT} = 215 K were found, when sulfuric acid tetrahydrate becomes liquid. Further information about the meteorological situation is given by *Dörnbrack et al.* [2002].

4. Flight Overview

[18] The balloon was launched on 25 January 2000 at 2000 UT from Esrange near Kiruna/Sweden. The first PSC encounter occurred during the first ascent at 21 km altitude

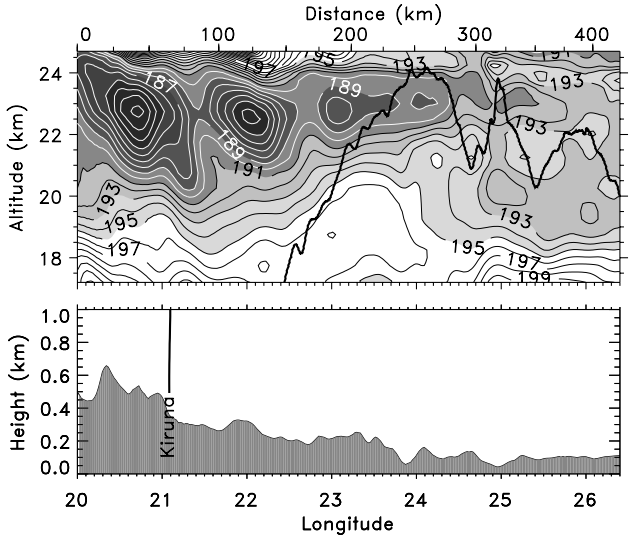

Figure 3. Vertical temperature cross section along the flight track on 25 January 2000 at 2200 UT, simulated with a mesoscale MM5-model [*Dörnbrack et al.*, 2002]. The mesoscale simulation with 2.6 km horizontal grid size, initialized on 25 January 2000 at 0600 UT was forced by global analysis at 0.5° × 0.5° resolution by the European Centre for Medium Range Weather Forecast (ECMWF). The black line indicates the balloon trajectory with several ascents and descents. The lower panel displays the orography below the balloon trajectory. The balloon launch was near Kiruna at 21.1° longitude.

at 74900 s UT (or 20.81 h UT). After reaching its float altitude above the PSCs near 24 km, the balloon operators repeatedly lowered and raised the balloon by releasing hydrogen and ballast, respectively. Each of the three ascents and descents between 20 and 24 km lasted for approximately 30 min. The PSC with a horizontal extension of more than 200 km was observed for over two hours at altitudes between 20 and 23 km (or between 475 and 540 K potential temperature). The temperature distribution shown in Figure 3 suggests that the PSC already existed upwind.

[19] Figure 4 presents a composite overview of the different measurements obtained during the flight as well as information derived during the analysis. PSCs are defined by backscatter ratios larger than 0.5 at 940 nm. Layers have been identified by correlated increases/decreases in the data of the individual instruments monitoring particle parameters that include the mass spectrometer signals (Figures 4a and 4b), the particle size and number concentration (Figure 4d), the backscatter data, and the depolarization (Figure 4f). The PSC particles existed at temperatures from 2 K below T_{ICE} to slightly above T_{NAT} (Figure 4h). Interestingly, the presence of PSC particles does not correlate with the lowest stratospheric temperatures. In contrast, under similar temperature, pressure, and water vapor conditions, PSCs were present in some cases and were not observed in others. The water vapor mixing ratio (Figure 4g) ranged between 5 and 7 ppmv at PSC altitudes, with small-scale variations of ±0.5 ppmv, which could be related to dynamic variations in air near the edge of the polar vortex. Details on the altitude range covered during the flight (Figure 4i) conclude the information presented in Figure 4.

5. PSC Particle Analysis

5.1. Introductory Remarks to the Analysis of ACMS Data

[20] The ACMS was designed to operate at pressures below 100 mbar, thus measurements started at 18 km altitude on the initial ascent and continued until the gondola was separated from the balloon after two hours. Particle water at mass 18 (H_2O^+) and HNO_3 at mass 63 (HNO_3^+) and 46 (NO_2^+, coming from HNO_3 fractionation during the ionization process and from decomposition on the wall of the evaporation sphere) were most frequently sampled, approximately every 2 s. Particle water and nitric acid (mass 63 only) are shown in Figures 4a and 4b, respectively. HNO_3 shows in the range of low count rates increasing discrete values. This pattern is a result of normalizing the counts measured in 250 ms to a rate of counts per second and applying corrections to the sensitivity of this particular mass channel. Signals at mass 46 were about 45 times larger than the signals at mass 63 shown in Figure 4. Both masses were used to calculate the total amount of HNO_3 contained in the sampled particles. The ACMS data showed that the time constant for the evolved gases to leave the small sphere was short for water vapor and longer for HNO_3 and NO_2. Between successive water measurements large signals decreased by over a factor of 20, when no more particles entered the system. In contrast, HNO_3 showed considerably slower changes in the measured count rates at mass 46 and mass 63 when the gondola entered or left a cloud layer. This is a result of adsorption and desorption processes, probably inside the evaporation sphere. Analysis of the HNO_3 data requires that these effects be carefully considered when calculating molar ratios. Particularly at the beginning of the measurements, when the first cloud layer was encountered, adsorption processes may have resulted in nitric acid signals below that carried by the particles. Aside from the first cloud measurements careful selection of time periods led to the determination of reliable molar ratios with reasonable uncertainties (see Figure 4c). Periods were selected in such a way that possible initial deficiencies in HNO_3 measurements and delayed decreases over a selected period were balanced-out. All other instrumental checks on sensitivity, stability and fragmentation of molecules such as HNO_3 showed that the instrument performed as predicted from laboratory calibration and preflight evaluations.

5.2. PSC Particle Analysis and Interpretation

[21] In the following a detailed description of the measurements shown in Figure 4, including comparisons and complementary information, is provided. Results of the analysis will be presented starting with more general conclusions and proceeding to detailed discussions of specific cloud features. Adsorption and desorption processes that were observed in HNO_3 and were discussed above have been considered in the molar ratios presented below.

[22] Closely correlated increases in the condensed water and the nitric acid data (Figures 4a and 4b) show that both species are indeed major components of PSC particles. As an estimate, an average count rate of 10000 s^{-1} of water on

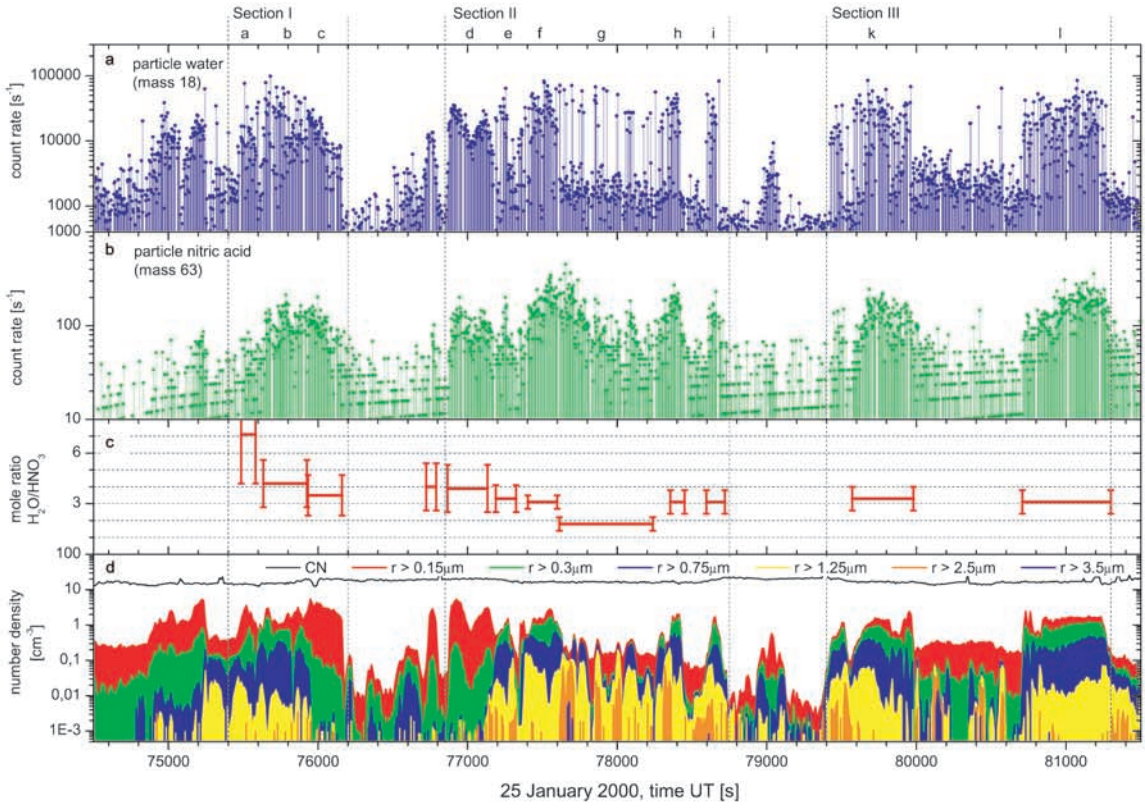
Section I
Section II
Section III
a b c d e f g h i k l
a particle water (mass 18)
count rate [s⁻¹]
b particle nitric acid (mass 63)
c
mole ratio H2O/HNO3
d CN r > 0.15µm r > 0.3µm r > 0.75µm r > 1.25µm r > 2.5µm r > 3.5µm
number density [cm⁻³]
75000 76000 77000 78000 79000 80000 81000
25 January 2000, time UT [s]

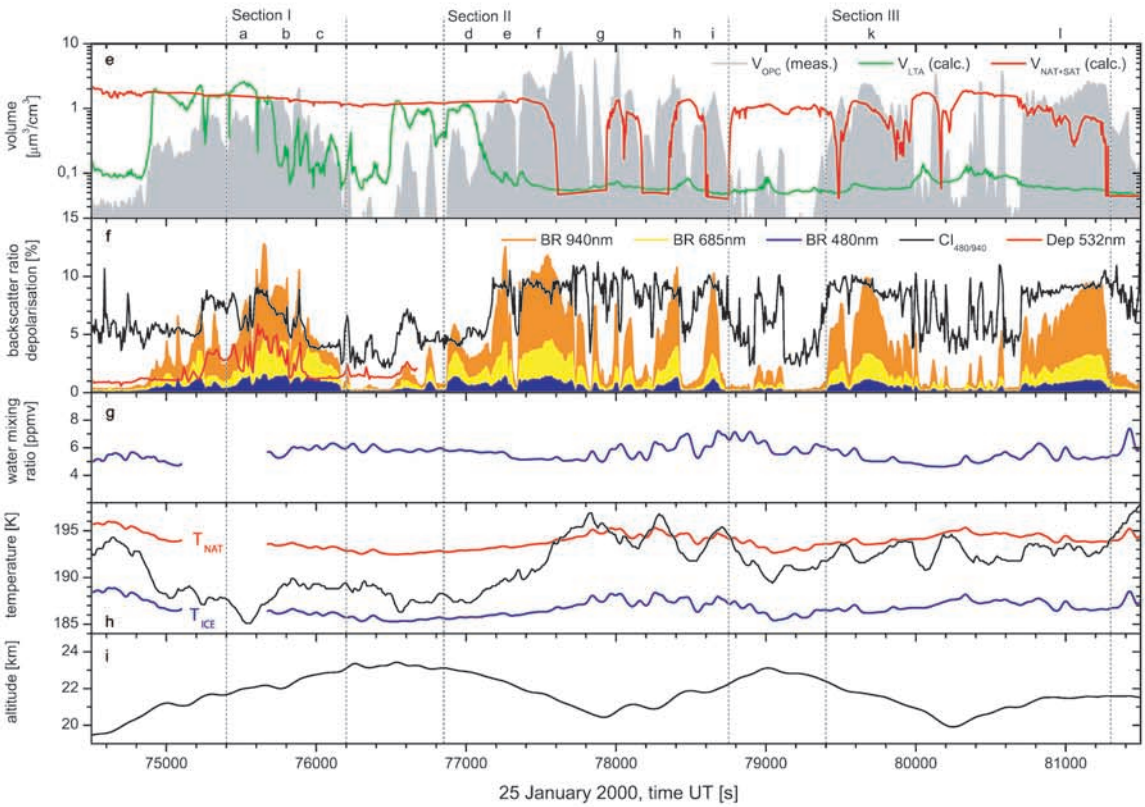
Section I
Section II
Section III
a b c d e f g h i k l
e
volume [µm²/cm³]
V_OPC (meas.) V_LTA (calc.) V_NAT+SAT (calc.)
f
backscatter ratio depolarisation [%]
BR 940nm BR 685nm BR 480nm CI480/940 Dep 532nm
g
water mixing ratio [ppmv]
temperature [K]
T_NAT
T_ICE
h
i
altitude [km]
75000 76000 77000 78000 79000 80000 81000
25 January 2000, time UT [s]

mass 18 (H_2O^+) in PSCs corresponds to 7 ± 2 ppbv water in the condensed phase as derived from the calibration. For an average count rate of 100 s^{-1} on mass 63 (HNO_3^+), the equivalent concentration of nitric acid in the condensed phase is 4 ± 1 ppbv.

[23] The most general information can be obtained when H_2O and HNO_3 signals are integrated over the entire flight from 74500 s to 81500 s (20.69 h to 22.64 h UT), for which a molar ratio of 3.1 ± 0.8 was determined. A more detailed picture emerges when the flight is divided into three sections I, II, and III that still permit integrations of the H_2O and HNO_3 signals from low levels near background to a similar low level after the gondola left a cloud layer. This should balance-out both surface effects in HNO_3 even for the early measurements. Section I ranges from 75400 to 76200 s UT and results in a molar ratio of 3.9 ± 1.0, section II from 76850 to 78750 s UT with a molar ratio of 2.5 ± 0.5 and, finally, section III from 79400 to 81300 s UT with a molar ratio of 3.2 ± 0.7. This information is provided to offer some clues as to which kind of particles might be present in any of the three sections.

[24] Some other more general features are found in the ACMS data between the PSC layers when condensed water count rates ranged only between 800 and 2000 s^{-1} corresponding to condensed water in aerosols ranging from 0.5 to 1.4 ppbv. These values are consistent with estimations derived from the particle counter data and from model calculations [*Carslaw et al.*, 1995] assuming aqueous sulfate particles in equilibrium with the gas phase. Of interest is the time period after section I between 76200 and 76500 s UT, when the balloon was located above the PSC layer near 24 km (25 mbar). During this period, the condensed water count rates correspond to approximately 1 ppbv particulate water, which can be attributed to sulfate background aerosols at the upper edge of the Junge layer. Although temperatures were as low as 5 K below T_{NAT}, neither NAT particles nor liquid ternary aerosols were observed. Very low particle volumes were found again at a similar high altitude after section II and before section III, when atmospheric temperatures were higher but still below T_{NAT}.

[25] A more detailed discussion of the results will start with section III in which two very distinct cloud layers were encountered with fewer particles present between the layers. The large water signals show many spikes, which are produced when single relatively large particles impacted the evaporation sphere. The atmospheric temperature during this period was high but always below T_{NAT}. When descending through the first of the two cloud layers (section III k), the gondola crossed the potential temperature of 508 K while the same potential temperature was reached again during the next ascent within the second cloud layer (III l). Although NAT particles were detected earlier during the flight, the very strong signals of H_2O and HNO_3 and the derived molar ratio of 3.3 ± 0.7 for the first and 3.1 ± 0.7 for the second cloud provide the best evidence to date on the presence of NAT particles in mountain wave PSCs.

[26] Backscatter ratios as well as particle size distribution are strongly correlated to the ACMS signals throughout section III. Within the NAT clouds the backscatter ratio ranges between 2 and 10. High color indices between 7 and 11 indicate larger, and therefore solid, particles. Both layers reveal a very similar pattern in size distribution. Particles with radii larger than 0.75 μm appear at concentrations up to 0.6 cm^{-3}. For cloud layer III k a bimodal lognormal particle size distribution has been fitted to the measured cumulative distribution and is shown in Figure 5. The large mode of the lognormal distribution shows a median radius of 0.75 μm with a sigma of 0.7 and a particle concentration of 0.55 cm^{-3}. This fit corresponds to a particle surface area of 5.8 μm^2 cm^{-3} and a volume of 1.6 μm^3 cm^{-3}. Approximately 20 min later when the balloon ascended through the second cloud (III l) returning to the same potential temperature, the large mode of the bimodal particle size distribution has now a median radius of 0.5 μm (sigma 0.8) at concentrations of 0.53 cm^{-3}.

[27] Turning now to the beginning of the measurements just before section I, a more complex picture is seen. Initially, the HNO_3 signal is low (up to 75600 s UT) which might be explained, in part, by a conditioning process of the ACMS system due to adsorption effects, while outgassing at the end of section I is observed. Nevertheless, the derived molar ratio of 3.9 for the entire section should be a good representation since both conditioning effects were accounted for. The atmospheric temperatures were the lowest of the entire flight and reached values as low as 185 K, which is well below T_{ICE}.

[28] Comparing the different cloud layers in more detail, the water signal distribution around I c is very smooth, indicating the presence of small particles with high number densities. Such particles would cause a steady gas flow into the mass spectrometer, which is different from the signals measured in section III k and l, when many spikes were observed. The data from the other instruments onboard the gondola support the proposition that liquid ternary aerosol (LTA) particles were present during I c near the temperature of 189 K. The optical particle counters showed a distinct change in particle size distribution at I c. Small particles (<0.5 μm) were measured at high number concentrations, but only a few large particles appeared. Further circumstantial evidence includes the low depolarization and the low color index. The same potential temperature of 530 K was crossed again in section II d when again a smooth signal distribution

Figure 4. (opposite) Chemical, microphysical and optical properties of PSCs measured on 25 January 2000 with balloonborne instrumentation. (a) Condensed phase water measured in the ACMS. (b) Condensed phase nitric acid. (c) Derived particle H_2O:HNO_3 molar ratios. (d) Integrated particle concentration in different size classes and concentration of condensation nuclei (black line) measured with OPC and CN counter. (e) Condensed phase volume (gray shaded area) measured with the optical particle counter (OPC), NAT+SAT volume (red line) and LTA volume (green line) calculated with an equilibrium model [*Carslaw et al.*, 1995] assuming 10 ppbv HNO_3, H_2O and H_2SO_4 were taken from measurements. (f) Backscatter ratios at three different wavelengths, depolarization (red line) and color index (black line). (g) Water vapor mixing ratio measured with the hygrometer. (h) Atmospheric temperature (black line), T_{ICE} (blue line) and T_{NAT} (red line), the latter calculated from the measured H_2O concentrations assuming 10 ppbv HNO_3. (i) Altitude.

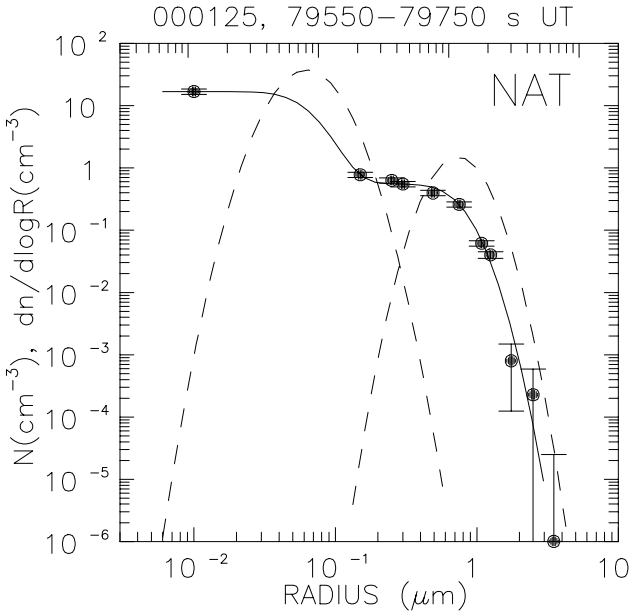

Figure 5. Bimodal lognormal size distributions fit to optical particle counter measurements (solid circles) in regions of the cloud that were identified as NAT. The data are averaged over the time interval 79550–79750 s. Uncertainties in the concentration measurements, due to counting errors, are represented by the error bars, which are limited to every other particle at low concentrations to limit confusion. The differential lognormal distributions for each mode are shown as dashed lines, and the cumulative concentration, from summing the integrals of the differential distributions, is shown as the solid line and should match the measurements for a good fit to the data. The parameters of the size distributions and the inferred surface areas and volumes are: NAT, N1 = 16 cm^{-3}, r1 = 0.065 μm, σ1 = 0.75, N2 = 0.55 cm^{-3}, r2 = 0.75 μm, σ2 = 0.75, Surface Area = 5.8 μm^2 cm^{-3}, Volume = 1.6 μm^3 cm^{-3}.

in the water measurements was found. Here the molar ratio was determined to be 3.9 ± 1.4 and the atmospheric temperature ranged between 187 and 189 K. Similar to the impressive demonstration of the presence of NAT particles in section III, the mass spectrometer data, particularly the water measurements, and results from the other instruments support the conclusion that LTA particles comprise the bulk of the particles in I c and II d at temperatures well below T_{NAT}.

[29] The LTA cloud layers at I c can be characterized by a median particle radius, for the small mode of the bimodal lognormal size distribution, of 0.05 μm with a sigma of 2.1 at a particle concentration of 20 cm^{-3} (Figure 6). Particle sizes were, however, changing as the balloon passed through this LTA region of the cloud. About 150 m below the size distribution shown in Figure 6, median radii were 0.1 μm and distribution widths 1.6. The gondola passed through a very similar cloud region at II d where the size distributions required median radii of 0.08 μm and widths of 1.6. Total particle concentrations were similar, 20 cm^{-3}.

[30] Considering the cloud layers before the LTA layer in section I, a different picture emerges: water signals show considerable structure and fluctuations over short altitude ranges. Spikes in the water measurement indicate the presence of relatively large single particles. The lowest temperature of 185 K is found at I a. During that part of the flight the depolarization signal is high, the OPC data show particles of radii larger than 1 μm, and the molar ratio was determined to be 7.1, but with a high uncertainty of ±2.9. This suggests that besides NAT particles ice particles were also present. The high color index in addition serves as indicator for larger, therefore solid, particles. Shortly after, the temperature increased above T_{ICE}, backscatter, depolarization, and color index decreased (I b). The molar ratio was determined to be 4.1 ± 1.4. This probably is marking a transition from ice/NAT to NAT/LTA particles.

[31] The most remarkable result of the balloon flight is found in section II. The beginning of this period (II d) has already been discussed and was identified as a cloud layer containing liquid particles observed near 530 K potential temperature. Following that and approaching 508 K, two cloud layers show water signals with numerous spikes (II e and f). The OPC measured a particle size distribution similar to the one found during NAT cloud encounters in section III. The molar ratios calculated for these periods were close to 3.0. Around II g, starting at 77600 s UT and lasting until 78350 s UT, a sequence of unusual water and HNO_3 signals was observed: water data show a few single particle impacts interspersed with a few sections with several large peaks together. Besides the water spikes detected with the ACMS many smaller water signals were continuously observed. Most impressive, however, are the large signals measured at mass 46 and 63 that cannot be explained with HNO_3 desorption processes. During this time, the maximum ambient temperature was as much as 2 K above T_{NAT}. The molar ratio for the entire period II g of 13 min was 2.0 or slightly below with some short periods

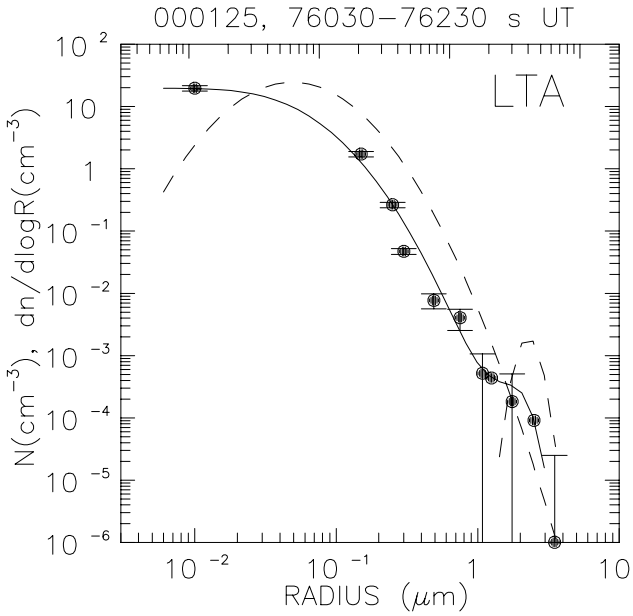

Figure 6. Same as Figure 6 for the time interval 76030–76230 s, a region of the cloud identified as LTA. The parameters of the size distributions and the inferred surface areas and volumes are: LTA, N1 = 20 cm^{-3}, r1 = 0.049 μm, σ1 = 1.05, N2 = 0.0003 cm^{-3}, r2 = 2.25 μm, σ2 = 0.6, Surface Area = 1.8 μm^2 cm^{-3}, Volume = 0.13 μm^3 cm^{-3}.

interspersed with molar ratios close to 3, where large water peaks are more numerous. While the amount of HNO_3 detected is similar to that found in NAT particles, there is, however, considerably less water present. This could be the first observation of nonequilibrium NAT particle evaporation. In this part of the flight the OPC measured a few (0.01 cm^{-3}) large particles with radii as high as 3.5 μm. These particles, however, cannot enter the ACMS system and thus are not measured by the mass spectrometer. Shortly after this, two small cloud layers, II h and i, show molar ratios near 3.0 when the temperature dropped again below T_{NAT} demonstrating that the generally accepted NAT temperature scale is a proper description for the existence of NAT particles.

[32] Condensed phase volumes have been derived from the particle counter data, shown in Figure 4e. NAT layers contain volumes of less than 3 $\mu m^3 cm^{-3}$, in contrast to layers of LTA particles that have less than 1 μm^3 cm^{-3}. In addition, these volumes have been compared to NAT and LTA volumes calculated with an equilibrium model [*Carslaw et al.*, 1995] using the measured water vapor, 0.2 ppbv sulfuric acid based on OPC data and 10 ppbv nitric acid (red and green line in Figure 4e). This panel shows clearly that, based on temperatures, LTA could only be expected between 74800 and 77200 s, and there is some agreement in the structure of the measured and modeled fluctuations in volume in this region, if not in the magnitudes. Figure 4e also shows very clearly regions of the cloud where, in equilibrium, PSCs should be present, yet none are observed.

[33] Comparisons with volumes derived from the ACMS data (not shown) reveal some discrepancies. In NAT cloud layers, the ACMS measures on the average 30% less condensed phase volume, which could be attributed to the reduced transmission of large nonspherical particles in the ACMS. In contrast, the ACMS volumes derived in LTA layers are on the average 40% larger compared to the OPC data. While this discrepancy is not yet understood, it might be explained by a partial evaporation of LTA particles in the inlet of the particle counter. In LTA layers, the ACMS data are in the range predicted by model calculations and the OPC data tend to be lower. Note that fast temperature changes in lee wave conditions can lead to nonequilibrium compositions and volumes of ternary particles due to differences in the timescales for water and nitric acid uptake or release. In NAT layers, there is rough agreement between both data sets and the model, considering the 30% error in both measurements and the uncertainty in the nitric acid gas phase. Furthermore, NAT particles might not be in equilibrium with the gas phase due to condensation and evaporation times for large particles.

6. Summary

[34] Properties of polar stratospheric cloud particles, which were processed by a mesoscale cold temperature region above Scandinavia, were extensively probed with a balloonborne set of instruments. The PSC consisted of many layers with different particle types, observed over a wide temperature range. During the first ascent through the cloud, ternary solution droplets were found at the top of the cloud at temperatures just above the ice frost point. The main body of the cloud consisted of layers containing NAT particles, which were stable up to the NAT equilibrium temperature. In the coldest region of the atmosphere encountered during the first ascent, solid particles were identified by high depolarization. High color index and backscatter ratios and large molar ratios derived from the ACMS data indicate the presence of ice and NAT particles. Later, however, the local atmospheric temperature exceeded T_{NAT} a number of times. Molar ratios determined during this period are well below 3.0. It appears that particles at the bottom of the cloud had no unusual amount of HNO_3, but considerably less water, and may present a first observation of evaporating NAT particles. Whenever the temperature again dropped below T_{NAT} during that time, large particles became more numerous and the molar ratio approached 3.0 again. A detailed microphysical modeling of the evolution of the NAT and LTA cloud layers is given in an accompanying paper by *Larsen et al.* [2002].

[35] **Acknowledgments.** The balloon flight was performed as part of the European-American SOLVE/THESEO 2000 campaign in winter 1999/2000. We like to acknowledge the excellent work of the balloon operation team from CNES. Fruitful discussions with T. Peter, B. Luo, and S. Füglistaler are gratefully acknowledged. This work has been supported by the Commission of the European Union through the Environment and Climate program (contracts ENV4-CT97-0523 and EVK2-CT-2000-00095). The work of T.D., C.K., J.R., and N.K. was supported by the U.S. National Science Foundation.

References

Adriani, A., F. Cairo, S. Mandolini, G. Di Donfrancesco, T. Deshler, and B. Nardi, A new joint balloon-borne experiment to study Polar Stratospheric Clouds: Laser Backscatter Sonde and Optical Particle Counter, in *Proceedings of XVIII Quadrennial Ozone Symposium, L'Aquila 1996, Atmospheric Ozone*, vol. 2, edited by R. D. Bojkov and G. Visconti, pp. 879–882, Edigrafital for Parco Sci. e Tecnol. d'Abruzzo, L'Aquila, Italy, 1998.

Browell, E. V., C. F. Butler, S. Ismail, P. A. Robinette, A. F. Carter, N. S. Higdon, O. B. Toon, M. R. Schoeberl, and A. F. Tuck, Airborne lidar observations in the wintertime Arctic stratosphere: Polar stratospheric clouds, *Geophys. Res. Lett.*, *17*, 385–388, 1990.

Carslaw, K. S., B. P. Luo, S. L. Clegg, T. Peter, P. Brimblecombe, and P. J. Crutzen, Stratospheric aerosol growth and HNO_3 gas phase depletion from coupled HNO_3 and water uptake by liquid particles, *Geophys. Res. Lett.*, *21*, 2479–2482, 1994.

Carslaw, K. S., B. Luo, and T. Peter, An analytic expression for the composition of aqueous HNO_3-H_2SO_4 stratospheric aerosols including gas phase removal of HNO_3, *Geophys. Res. Lett.*, *22*, 1877–1880, 1995.

Carslaw, K. S., M. Wirth, A. Tsias, B. P. Luo, A. Dörnbrack, M. Leutbecher, H. Volkert, W. Renger, J. T. Bacmeister, and T. Peter, Particle microphysics and chemistry in remotely observed mountain polar stratospheric clouds, *J. Geophys. Res.*, *103*, 5785–5796, 1998.

Carslaw, K. S., T. Peter, J. T. Bacmeister, and S. D. Eckermann, Widespread solid particle formation by mountain waves in the Arctic stratosphere, *J. Geophys. Res.*, *104*, 1827–1836, 1999.

Crutzen, P. J., and F. Arnold, Nitric acid cloud formation in the cold Antarctic stratosphere: A major cause for the springtime "ozone hole", *Nature*, *324*, 651–655, 1986.

David, D., S. Godin, G. Megie, Y. Emery, and C. Flesia, Physical state and composition of polar stratospheric clouds from airborne lidar measurements during SESAME, *J. Atmos. Chem.*, *27*, 1–16, 1997.

Del Negro, L. A., et al., Evaluating the role of NAT, NAD, and liquid H_2SO_4/HNO_3/H_2O solutions in Antarctic polar stratospheric cloud aerosol: Observations and implications, *J. Geophys. Res.*, *102*, 13,255–13,282, 1997.

Deshler, T., and S. J. Oltmans, Vertical profiles of volcanic aerosol and polar stratospheric clouds above Kiruna, Sweden: Winters 1993 and 1995, *J. Atmos. Chem.*, *30*, 11–23, 1998.

Deshler, T., B. Nardi, A. Adriani, F. Cairo, G. Hansen, F. Fierli, A. Hauchecorne, and L. Pulvirenti, Determining the index of refraction of polar stratospheric clouds above Andoya by combining size-resolved concentration and optical scattering measurements, *J. Geophys. Res.*, *105*, 3943–3953, 2000.

Dörnbrack, A., T. Birner, A. Fix, H. Flentje, A. Meister, H. Schmid, E. V.

Browell, and M. J. Mahoney, Evidence for inertia gravity waves forming polar stratospheric clouds over Scandinavia, *J. Geophys. Res.*, *107*(D20), 8287, doi:10.1029/2001JD000452, 2002.

Drdla, K., A. Tabazadeh, R. P. Turco, M. Z. Jacobson, J. E. Dye, C. Twohy, and D. Baumgardner, Analysis of the physical state of one Arctic polar stratospheric cloud based on observations, *Geophys. Res. Lett.*, *21*, 2475–2478, 1994.

Dye, J. E., B. W. Gandrud, D. Baumgardner, L. Sanford, and G. V. Ferry, A survey of particle measurements in the Arctic from the Forward Scattering Spectrometer Probe Model 300, *Geophys. Res. Lett.*, *17*, 409–412, 1990.

Fahey, D. W., K. K. Kelly, G. V. Ferry, L. R. Poole, J. C. Wilson, D. M. Murphy, M. Lowenstein, and K. R. Chan, In situ measurements of total reactive nitrogen, total water, and aerosol in a polar stratospheric cloud in the Arctic, *J. Geophys. Res.*, *94*, 11,299–11,315, 1989.

Fahey, D. W., K. K. Kelly, S. R. Kawa, A. F. Tuck, M. Lowenstein, K. R. Chan, and L. E. Heidt, Observations of denitrification and dehydration in the winter polar stratosphere, *Nature*, *344*, 321–324, 1990.

Fahey, D. W., et al., The detection of large HNO_3 particles in the winter Arctic stratosphere, *Science*, *291*, 1026–1031, 2001.

Hanson, D., and K. Mauersberger, Laboratory studies of the nitric acid trihydrate: Implications for the south polar stratosphere, *Geophys. Res. Lett.*, *15*, 855–858, 1988.

Koop, T., K. S. Carslaw, and T. Peter, Thermodynamic stability and phase transitions of PSC particles, *Geophys. Res. Lett.*, *24*, 2199–2202, 1997.

Larsen, N., B. M. Knudsen, J. M. Rosen, N. T. Kjome, R. Neuber, and E. Kyrö, Temperature histories in liquid and solid polar stratospheric cloud formation, *J. Geophys. Res.*, *102*, 23,505–23,517, 1997.

Larsen, N., I. S. Mikkelsen, B. M. Knudsen, J. Schreiner, C. Voigt, K. Mauersberger, J. M. Rosen, and T. Kjome, Comparison of chemical and optical in situ measurements of polar stratospheric cloud particles, *J. Geophys. Res.*, *105*, 1491–1502, 2000.

Larsen, N., et al., Microphysical mesoscale simulations of polar stratospheric cloud formation constrained by in situ measurements of chemical and optical could properties, *J. Geophys. Res.*, *107*, doi:10.1029/2001JD000999, in press, 2002.

Meilinger, S. K., T. Koop, B. P. Luo, T. Huthwelker, K. S. Carslaw, U. Krieger, P. J. Crutzen, and T. Peter, Size-dependent stratospheric droplet composition in mesoscale temperature fluctuations and their potential role in PSC freezing, *Geophys. Res. Lett.*, *22*, 3031–3034, 1995.

Ovarlez, J., and H. Ovarlez, Stratospheric water vapor content evolution during EASOE, *Geophys. Res. Lett.*, *21*, 1235–1238, 1994.

Ovarlez, J., and H. Ovarlez, Water vapor and aerosols measurements during SESAME, and the observation of low water vapor content layers, in *Air Pollution Report 56 on Polar Stratospheric Ozone*, pp. 205–208, Eur. Comm., Brussels, 1996.

Rosen, J. M., and N. T. Kjome, Backscattersonde: A new instrument for atmospheric aerosol research, *Appl. Opt.*, *30*, 1552–1561, 1991.

Schiller, C., et al., Dehydration in the Arctic stratosphere during the SOLVE/THESEO 2000 campaigns, *J. Geophys. Res.*, *107*(D20), 8293, doi:10.1029/2001JD000463, 2002.

Schreiner, J., C. Voigt, K. Mauersberger, P. McMurry, and P. Ziemann, Aerodynamic lens system for producing particle beams at stratospheric pressures, *Aerosol Sci. Technol.*, *29*, 50–56, 1998.

Schreiner, J., U. Schild, C. Voigt, and K. Mauersberger, Focusing of aerosols into a particle beam at pressures from 10 to 150 Torr, *Aerosol Sci. Technol.*, *31*, 373–382, 1999a.

Schreiner, J., C. Voigt, A. Kohlmann, F. Arnold, K. Mauersberger, and N. Larsen, Chemical analysis of polar stratospheric cloud particles, *Science*, *283*, 968–970, 1999b.

Schreiner, J., C. Voigt, P. Zink, A. Kohlmann, D. Knopf, C. Weisser, P. Budz, and K. Mauersberger, A mass spectrometer system for analysis of polar stratospheric aerosols, *Rev. Sci. Instrum.*, *73*, 446–452, 2002.

Tabazadeh, A., R. P. Turco, and M. Z. Jacobson, A model for studying the composition and chemical effects of stratospheric aerosols, *J. Geophys. Res.*, *99*, 12,897–12,914, 1994.

Toon, O. B., P. Hamill, R. P. Turco, and J. Pinto, Condensation of HNO_3 and HCl in the winter polar stratospheres, *Geophys. Res. Lett.*, *13*, 1284–1287, 1986.

Toon, O. B., E. V. Browell, S. Kinne, and J. Jordan, An analysis of lidar observations of polar stratospheric clouds, *Geophys. Res. Lett.*, *17*, 393–396, 1990.

Toon, O. B., A. Tabazadeh, E. V. Browell, and J. Jordan, Analysis of lidar observations of Arctic polar stratospheric clouds, *J. Geophys. Res.*, *105*, 20,598–20,615, 2000.

Voigt, C., Balloon-borne composition measurements of polar stratospheric clouds, Ph.D. thesis, 143 pp., Univ. of Heidelberg, Dec., 2000.

Voigt, C., et al., NAT in Polar Stratospheric Clouds, *Science*, *290*, 1756–1758, 2000a.

Voigt, C., S. Tsias, A. Dörnbrack, S. Meilinger, B. P. Luo, J. Schreiner, N. Larsen, K. Mauersberger, and T. Peter, Non-equilibrium compositions of liquid polar stratospheric clouds in gravity waves, *Geophys. Res. Lett.*, *27*, 3873–3876, 2000b.

World Meteorological Organization (WMO), *Scientific Assessment of Ozone Depletion, 1998*, Global Ozone Res. and Monit. Proj., Geneva, 1999.

Worsnop, D., L. E. Fox, M. S. Zahniser, and S. C. Wofsy, Vapor pressures of solid hydrates of nitric acid: Implication for polar stratospheric clouds, *Science*, *259*, 71–74, 1993.

Zink, P., D. Knopf, J. Schreiner, K. Mauersberger, O. Möhler, H. Saathoff, M. Seifert, R. Tiede, and U. Schurath, Cryo-chamber simulation of stratospheric H_2SO_4/H_2O particles: Composition analysis and model comparison, *Geophys. Res. Lett.*, *29*, doi:10.1029/2001GL013296, 2002.

A. Adriani, F. Cairo, and G. Di Donfrancesco, Istituto per la Scienza dell'Atmosfera e del Clima, Sezione di Roma, Via Fosso del Cavaliere 100, I-00133 Rome, Italy. (Alberto.Adriani@ifa.rm.cnr.it; cairo@ifa.rm.cnr.it; didonfra@sung3.ifsi.rm.cnr.it)

T. Deshler and C. Kröger, Department of Atmospheric Science, University of Wyoming, P.O. Box 3038, Laramie, WY 82071, USA. (deshler@uwyo.edu; ckroger@uwyo.edu)

A. Dörnbrack, Institute for Physics of the Atmosphere, DLR Oberpfaffenhofen, D-82234 Wessling, Germany. (andreas.doernbrack@dlr.de)

A. Kohlmann, K. Mauersberger, J. Schreiner, C. Voigt, and C. Weisser, Division of Atmospheric Physics, Max-Planck-Institute for Nuclear Physics, P.O. Box 103980, D-69029 Heidelberg, Germany. (Konrad.Mauersberger@mpi-hd.mpg.de; Jochen.Schreiner@mpi-hd.mpg.de; Christiane.Voigt@mpi-hd.mpg.de; Christoph.Weisser@mpi-hd.mpg.de)

N. Larsen, Division of Middle Atmospheric Research, Danish Meteorological Institute, Lyngbyvej100, DK-2100 Copenhagen, Denmark. (niels.larsen@dmi.dk)

J. Ovarlez and H. Ovarlez, Laboratoire de Meteorologie Dynamique, UMR 8539, F-91128 Palaiseau, France. (ovarlez@lmdx.polytechnique.fr)